Archives of Civil and Mechanical Engineering (2021) 21:111
https://doi.org/10.1007/s43452-021-00263-x

ORIGINAL ARTICLE

Analysis of thickness variation and stress state in hydroforming of complex T-shaped tubular part of nickel-based superalloy

Xiao-Lei Cui[1,2] · **Shijian Yuan**[1]

Received: 24 December 2020 / Revised: 27 May 2021 / Accepted: 24 June 2021 / Published online: 3 July 2021
© Wroclaw University of Science and Technology 2021

Abstract

Stress states on a multi-branch tubular part are the most complicated change in all types of hydroforming process, which result in severe variation of thickness. In this paper, an experimental and numerical research was conducted on a multi-step hydroforming process including intermediate annealing treatment to obtain effect of stress state on the thickness variation of a superalloy GH4169 complex T-shaped tubular part with expanded diameter, which corresponds to a real product used in aerospace industry. The material flow behavior at typical points on hydroformed tube blank was first analyzed. Then, the thickness variation on the hydroformed GH4169 tube blanks was discussed in every step. It is shown that the materials have different flow directions to form the side branch, where the thickness is always thinned during the four-step hydroforming process. Large axial feeding induces a continuous thickening between transition areas and tube ends. The thickness invariant dividing line in the side branch zone moves toward the tube ends with forming going on. However, in the hemisphere zone, it moves slightly towards the center of the side branch. Moreover, the stress states at three typical positions, as well as their effect on the thickness variation, were analyzed based on a sequential correspondence law between stress and strain components. On this basis, the mechanism of thickening in the left transition area, thinning at the top of side branch and thickness variation at the hemispheric pole was revealed. These results are very important for obtaining the thickness distribution of a complex T-shaped tubular part in multi-step hydroforming, and revealing the thickness variation mechanism by using engineering plasticity theory.

Graphic abstract

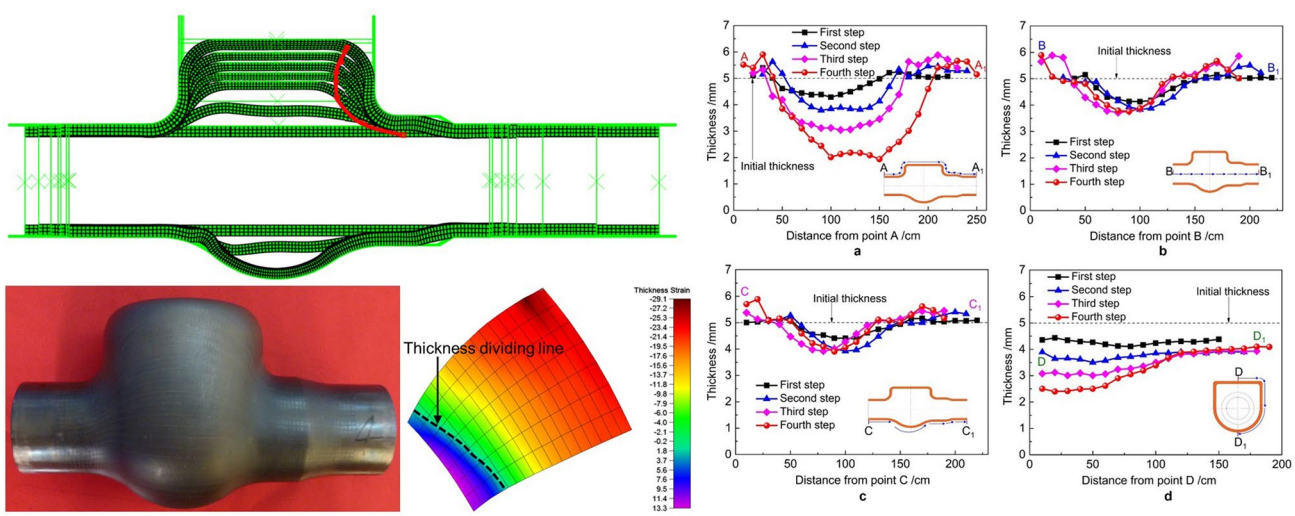

Keywords Hydroforming · Complex T-shaped tubular part · Thickness distribution · Stress · Nickel-based superalloy

Extended author information available on the last page of the article

1 Introduction

Nickel-based superalloys are commonly used in the key components of aerospace engines and gas turbines given their excellent mechanical properties, favorable oxidation resistance, and fatigue resistance in high-temperature environment [1]. To achieve lightweight and high reliability, many superalloy thin-walled components are used as engine piping system, air inlets, exhaust air duct, and so on. For example, T-shaped tubular part of superalloy is an important pipe joint of the aerospace engines. Hydroforming is an advanced forming technology for manufacturing thin-walled components with varied cross sections, which has gained great development in recent years [2]. Therefore, the hydroforming process is a good choice for the forming of T-shaped tubular parts of superalloy.

Generally, according to diameter difference between main tube and side branch, the T-shaped tubular parts can be divided into three categories: equal diameter, reduced diameter, and expanded diameter. Up to present, many investigations regarding the hydroforming of T-shaped tubular part with equal diameter and reduced diameter have been conducted. Ray et al. [3] used tube hydroforming process to form a simple T-shaped tubular part with equal diameter. They found that the developed height of side branch and the thickness distribution were in good agreement with experimental results. Crapps et al. [4] presented a parametric finite element analysis on hydroforming process of T-shaped tube with equal diameter for side branch using a history-dependent internal state variable model. Zadeh et al. [5] made a numerical simulation and experiment of the tube hydroforming of unequal T shapes with different branch diameters smaller than of the main tube, and finally, the reasonable loading paths were determined. Hwang et al. [6] proposed an adaptive control algorithm to determine appropriate loading paths in T-shaped tube hydroforming with different outlet diameters not larger than that of the main tube. Moreover, a design guideline for die surface shapes in T-shaped magnesium alloys tube hydroforming was also proposed by Hwang et al. [7]. However, hydroforming of T-shaped tubular part with expanded diameter still faces severe challenges because of its complexity and larger expansion ratio. Especially for the hard-to-deform nickel-based superalloys, it is not possible to obtain the expanded side branch using conventional one-step hydroforming process at room temperature. To overcome these difficulties, a multi-step hydroforming process at room temperature followed by intermediate annealing treatment was recently proposed by our research group to manufacture the complex superalloy T-shaped tubular part with expanded diameter [8].

It is well known that change of stress states on multi-branch tubular part is the most complex in all types of hydroforming process, which affects not only the forming defect form but also the thickness variation. For thin-walled components, the thickness uniformity is the most important technical indicator. In the position with most severe thickness thinning, it is usually subjected to a large tensile stress. Therefore, it is very important to study the effect of stress state on the thickness. Based on this, the stress state at the most severe thickness thinning position can be adjusted by changing the blank shape or the loading scheme, which can further improve the thickness uniformity [9]. In tube hydroforming, the thickness reduction should be as small as possible. In this case, analysis of the thickness variation and the stress state on both sides of the thickness invariant dividing line is essential. Cheng et al. [10] analyzed the thickness distribution of a Y-shape tube during the hydroforming process. It is found that the maximum thickness occurs in the leftward fillet transition region, rightward takes the second place, and the top of the side branch is the thinnest. With the increase of internal pressure, the biggest thickening ratio is not obviously changed; however, the maximum thinning ratio increased significantly. As the height of the side branch increases, an over-thinning and even splitting on the top of side branch will be caused [11]. Guo et al. [12] investigated the effects of the loading path and the friction coefficient on the side branch height and the thinning ratio distribution of Y-shapes. Their results demonstrated that the maximum thickening ratio occurred near the right transition fillet of Y-shapes. Moreover, the maximum thinning ratio was 11.92% and the side branch height was 90.3 mm. Peng et al. [13] proposed a multistage punch to change the internal pressure distribution in the guiding zone and to reduce the friction force between the tube and the die. Hence, the thickening ratio in the guiding zone is reduced by 20% and the thinning ratio of the side branch is reduced by 6%. Moreover, Hwang et al. investigated the thickness distribution of T-shape [14] and Y-shape [15] magnesium alloy tubular parts in hydroforming process at elevated temperatures of 150 ℃ and 250 ℃ by comparing the simulation and experimental results. Lei et al. [16] introduced the Oyane's ductile fracture integral to predict that the maximum thinning and bursting failure is located at the tip of side branch of a T-shaped tube in hydroforming. Lorenzo et al. [17] developed a proper optimization strategy on Y-shaped tube hydroforming process to increase as much as possible the bulge height of the Y-region obtained at the end of the process also guaranteeing the minimal thinning on the tube. In addition, Rajenthirakumar [18] first investigated the hydroforming process of Inconel 625 superalloy tube with equal diameter through numerical simulation and experiment, and the effects of strain hardening exponent, friction coefficient and normal anisotropic coefficient on thickness distribution were analyzed.

It can be seen from above overview that most of the investigations focus on the analysis of thickness distribution and the effect of process parameters. The effect of stress state on the thickness variation in the hydroforming process of a tee tube, especially the tubular parts with expanded diameter, has not been investigated so far. Compared with T-shaped tubular part with equal and reduced diameter, the superalloy tubular parts with expanded diameter are more difficult to be hydroformed, and the stress state and thickness variation are more complex. Therefore, it is urgent to investigate the thickness distribution and its relationship with stress state in the hydroforming process of a complex T-shaped tubular part with expanded diameter.

In this paper, the thickness variation and stress state of a complex T-shaped tubular part of nickel-based superalloy with expanded diameter was investigated during a four-step hydroforming process. The hydroformed tube blanks after every step were first given, on which the material flow behavior at typical positions was analyzed. Then, the thickness distribution of several typical sections on the hydroformed complex GH4169 T-shaped tubular part was given. Finally, the relationships between the thickness variation and stress state, as well as the stress state and the strain distribution patterns at typical position, were all discussed in detail.

2 Specimen and experimental procedure

2.1 Specimen and materials

Figure 1 shows the geometric shape and dimension of a complex T-shaped tubular part with expanded diameter, which corresponds to a real product used in aerospace industry. It has a side branch with larger diameter than that of the main tube and a varied diameter zone, which leads to it being an asymmetric structure along left–right and up–down directions. The outer diameters of the main tube and the varied diameter zone are 52.3 mm and 60.2 mm, respectively. The side branch has an outer diameter of 90.6 mm, which is 1.732 times the diameter of the main tube. Moreover, a hemisphere zone with radius of 45.3 mm is located at the bottom of side branch. The transition fillet radius between the main tube and the side branch is 14 mm, while that between the varied diameter zone and the side branch is 10 mm.

The complex T-shaped tubular parts will be manufactured using nickel-based superalloy GH4169 tubes, whose outer diameter and nominal thickness are 52.3 mm and 5.0 mm, respectively. The chemical composition of the GH4169 superalloy is given in Table 1 based on Chinese standard GB/T 14,992-2005. Mechanical properties of the GH4169 tube along axial direction were tested at room temperature using an Instron 5569 uniaxial tensile test machine. Figure 2 shows the true stress–strain curve, which tends to follow an ideal elastic-plastic linear hardening model. Moreover, the

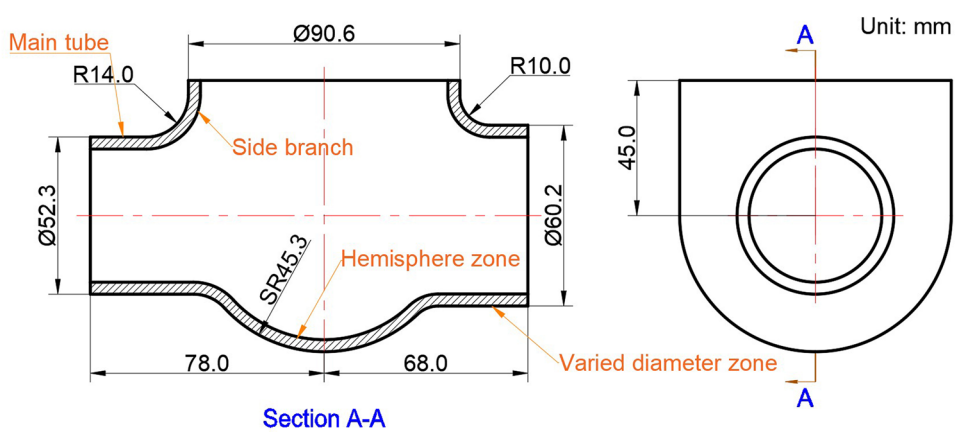

Fig. 1 Geometric shape and dimension of the complex T-shaped tubular part with expanded diameter

Table 1 Standard chemical composition of GH4169 superalloy (wt. %) [19]

Composition	C	Cr	Ni	Co	Mo	Al	Ti	Nb
Standard content	≤0.08	17.00–21.00	50.00–55.00	≤1.00	2.80–3.30	0.20–0.80	0.65–1.15	4.75–5.50
Composition	Fe	B	Mg	Mn	Si	P	S	Cu
Standard content	Bal.	≤0.006	≤0.010	≤0.35	≤0.35	≤0.015	≤0.015	≤0.300

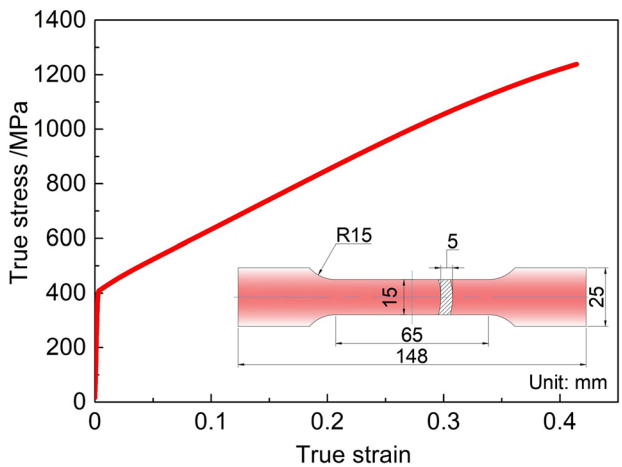

Fig. 2 True stress-strain curve of nickel-based superalloy GH4169 tube along the axial direction

Table 2 Mechanical property parameters of nickel-based superalloy GH4169 tube

Mechanical parameters	Value
Yield stress, σ_s (MPa)	414
Tensile strength, σ_b (MPa)	818
Total elongation, δ_u (%)	60.0
Uniform elongation, δ (%)	51.4

mechanical property parameters of the nickel-based superalloy GH4169 tube along the axial direction are listed in Table 2.

2.2 Multi-step hydroforming process

In Fig. 1, the larger diameter of the side branch than that of the main tube will result in an expansion ratio of 116.2%, which is far beyond the plasticity limit of the GH4169 superalloy tube at room temperature. Therefore, the complex T-shaped tubular part must be manufactured using a multi-step hydroforming process, as shown in Fig. 3a. During the multi-step hydroforming process, every hydroforming step was conducted at room temperature (RT) in the same hydroforming tool shown in Fig. 3b. Moreover, an annealing treatment obeying the process shown in Fig. 3c is essential to regain the ductility of the tube blank after every hydroforming step. During every annealing process, the tube blanks are placed in a furnace and heated to 600 ℃ for about 10 min, then continued to 900 ℃ for about 10 min and kept at 1020 ℃ for about 20 min. The purpose of holding at 600 ℃, 900 ℃ and 1020 ℃ is to dissolve the γ" phase, γ' phase, and δ phase into the matrix phase as fully as possible [20].The maximum heating temperature is 10 ℃ higher than the 1010 ℃ recommended in Chinese machinery industry standard JB/T 7712-2007, while the holding time is 20 min which chooses the lower limit of the recommended range of 20–45 min in the standard. Argon gas is then rapidly filled into the furnace to lower the temperature of tube blank to 500 ℃ quickly, which is followed by a furnace cooling to room temperature.

2.3 Experimental scheme

Experiments for manufacturing the nickel-based superalloy GH4169 T-shaped tubular part were conducted on a 3150 kN tube hydroforming machine. Table 3 shows the reasonable process parameters for the four-step hydroforming process of the T-shaped tubular part obtained from our previous investigation [8]. In the experiments, the as-received GH4169 tubes were first cut into tube blanks with a length of 300 mm, which were then placed in the die cavity for hydroforming. During every hydroforming step, the axial feeding of three punches and the internal pressure inside the tube blank can be controlled precisely according to the process parameters previously set in the computer-control system. After every hydroforming step, the thickness distributions are measured at intervals of 10 mm using a micrometer along several typical paths. Moreover, the strain distributions in several typical positions on the hydroformed tube blank will be measured by a grid analysis method. To measure the strain, square grid with size of 2 × 2 mm should be first printed on the initial tube blank using electrochemical etching. After hydroforming, a camera is used to take two or more photographs of the measurement area from two different angles. Finally, the photographs are imported into the ASAME software, and the strain distribution on the measurement area can be obtained after certain analysis.

2.4 Finite element modeling

To investigate the material flow behavior and the stress and strain distribution during the four-step hydroforming process of the GH4169 T-shaped tubular part, finite element simulation was conducted using the ABAQUS/Explicit software. Figure 4 shows the established three-dimensional (3D) finite element model, which consist of the die, the left punch, the right punch, the middle punch and the tube. The die, the left punch, the right punch and the middle punch were designed to be discrete rigid shells, while the tube was designed as a 3D deformable solid. The C3D8R elements (an 8-node linear brick, reduced integration, hourglass control) were assigned to the tube, and it was divided into 33,750 elements. In addition, the process parameters shown in Table 3 were used in the numerical simulations. Because the deformed tube blank after each hydroforming step was fully annealed in the experiment to restore its ductility, as shown in Fig. 3,

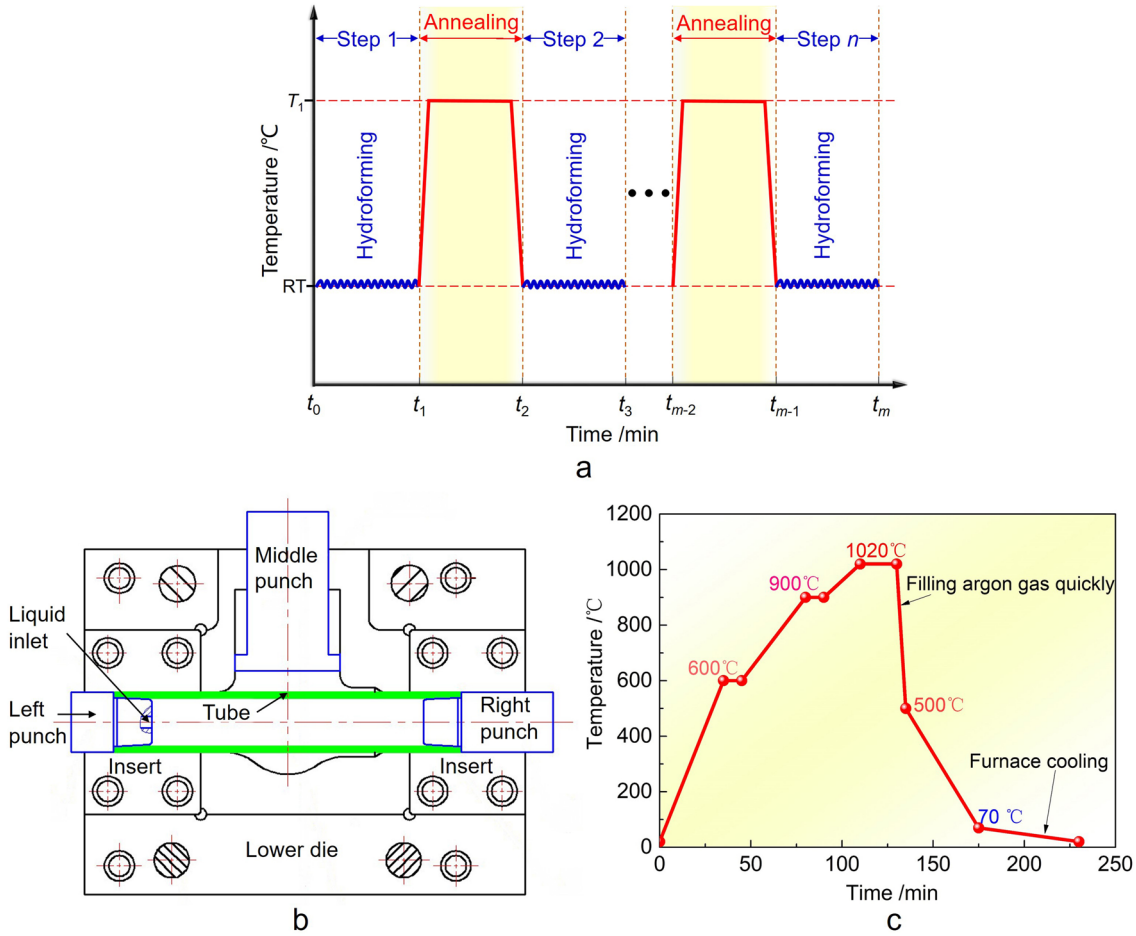

Fig. 3 Principle of multi-step hydroforming process for complex T-shaped tubular part of nickel-based superalloy [8]: **a** forming process, **b** hydroforming tool, **c** annealing process

Table 3 Process parameters for the four-step hydroforming of nickel-based superalloy GH4169 T-shaped tubular part [8]

Hydroforming step number	1	2	3	4
Internal pressure/MPa	80→170	80→160	80→200	80→200
Total axial feeding length/mm	60	25	12	9
Axial feeding ratio λ	4	4	1.4	3.5
Axial feeding length of left punch/mm	12	5	5	2
Axial feeding length of right punch/mm	48	20	7	7
Retreating displacement of middle punch/mm	18	7	8	6

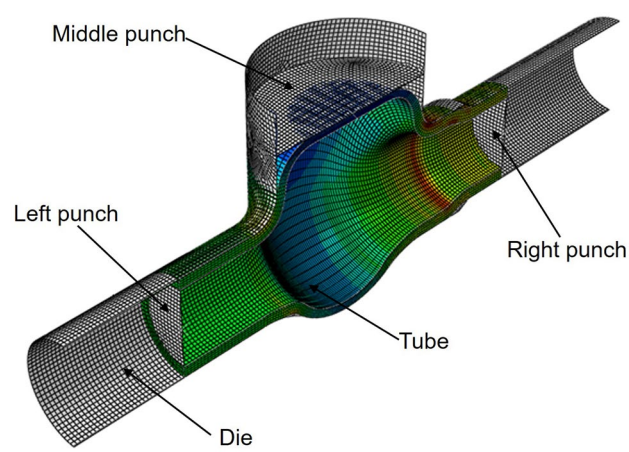

Fig. 4 Finite element model for the hydroforming of the complex GH4169 T-shaped tubular part [8]

it is possible to assume that the mechanical properties of the tube blank were restored to its initial state after each step. Therefore, in the numerical simulations, the mechanical properties related to initial tube material were taken for all steps of hydroforming.

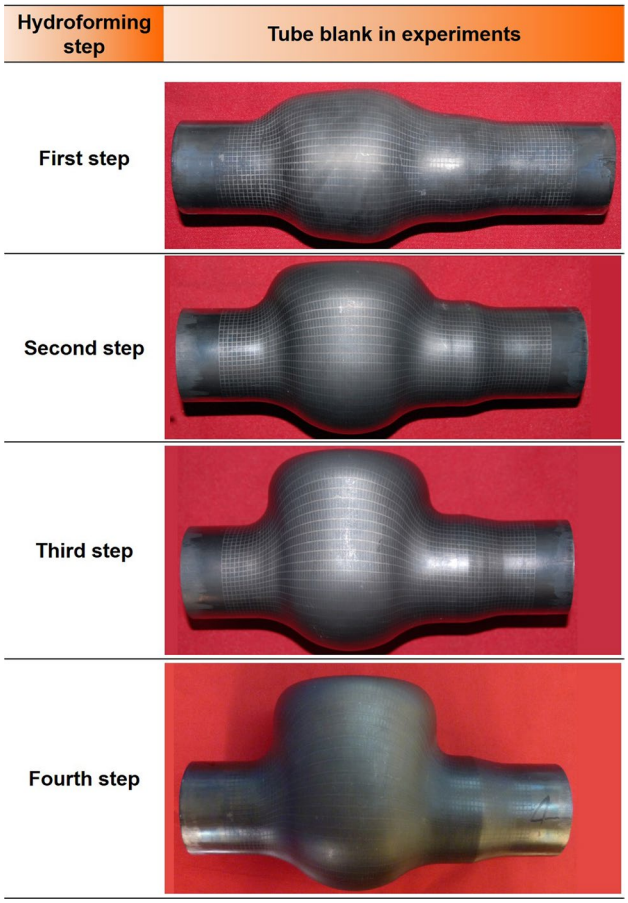

Fig. 5 Four-step hydroforming experimental results of complex GH4169 T-shaped tubular part

3 Results

3.1 Hydroforming process and the tube blank

Figure 5 shows the four-step hydroforming experimental results of complex GH4169 T-shaped tubular part. It can be seen from Fig. 5 that the side branch has not been formed at the end of the first step. Only a varied diameter tube blank was formed, and the diameter on the right side of deformation zone is larger than that on the left side. When the second step is completed, the side branch has been formed. In the third and fourth steps, the height of the side branch increases gradually, and the radius of the corner area at the top of the side branch decreases gradually. The experimental results show that after four steps of hydroforming, the tube blank can be completely attached to the die cavity.

3.2 Materials flow behavior at typical points in forming process

To analyze the material flow behavior during the hydroforming process of the complex GH4169 T-shaped tubular part, the flow trajectories at four typical points on left corner, top center, right corner and front corner of the side branch obtained by numerical modeling are shown in Fig. 6. The selected typical points on the left corner, the right corner and the top center are all located on the symmetric surface of the main tube.

It can be seen from Fig. 6a that the left corner is formed by the upward flow of the material in the deformation area. In the first step of hydroforming, the material basically flows vertically upward, and then deviates to the left due to the larger axial feeding length on right side than that of the left

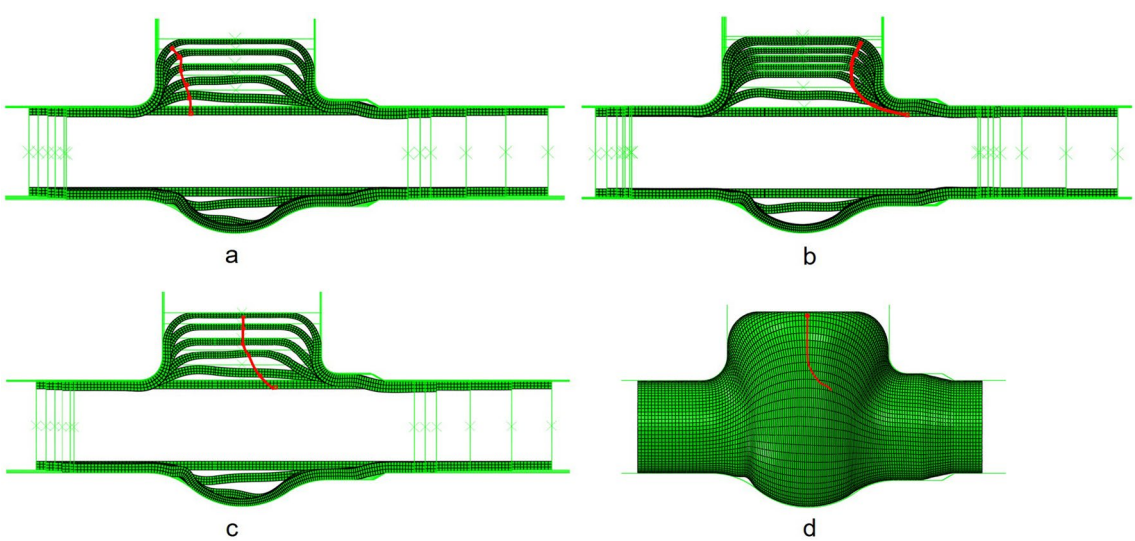

Fig. 6 Flow trajectory of typical points at the top of the side branch in forming process: **a** left corner, **b** right corner, **c** top center, **d** front corner

side. In the subsequent hydroforming steps, the material continues to deviate to the left under the action of axial feeding and internal pressure until it flows to the left corner of the side branch.

It can be seen from Fig. 6b that the material not only has a long flow distance, but also has a big change in direction for arriving the right corner due to the greater axial feeding length on the right side. In the first and second steps of hydroforming, the material flow is mainly controlled by axial force due to the relatively larger axial feeding of right punch, so it flows towards the upper left. Then, the material moves vertically upward under the equilibrium action of internal pressure and axial force. In the final stage, the material flow is significantly affected by internal pressure and it flows outward along radial direction of the side branch, so its flow direction begins to shift to the right.

In Fig. 6c, d, typical points on the top center and the front corner of the side branch have similar flow characteristic, both of which shift to the left and up first, and then flow vertically upward again. The difference is that the top center point moves in the symmetry plane while the point at the front corner moves in a 3D path. This is also because of the larger axial feeding on the right side in the early stage, which will cause the flow of material to the left side. In the later steps, the action of axial force is weakened, and the material moves vertically upward under the internal pressure.

3.3 Thickness distribution

Figure 7 shows the thickness distribution of several typical sections on the hydroformed GH4169 T-shaped tubular part with expanded diameter which are obtained experimentally. After the first step of hydroforming, the thickness distributions on paths of A-A_1, B-B_1 and C-C_1 indicate that thickening is the most severe in the left and right transition areas. The thickness in the zone between the transition area and the tube ends increases to different degrees. Thickness thinning zone is between the transition areas on both sides. On

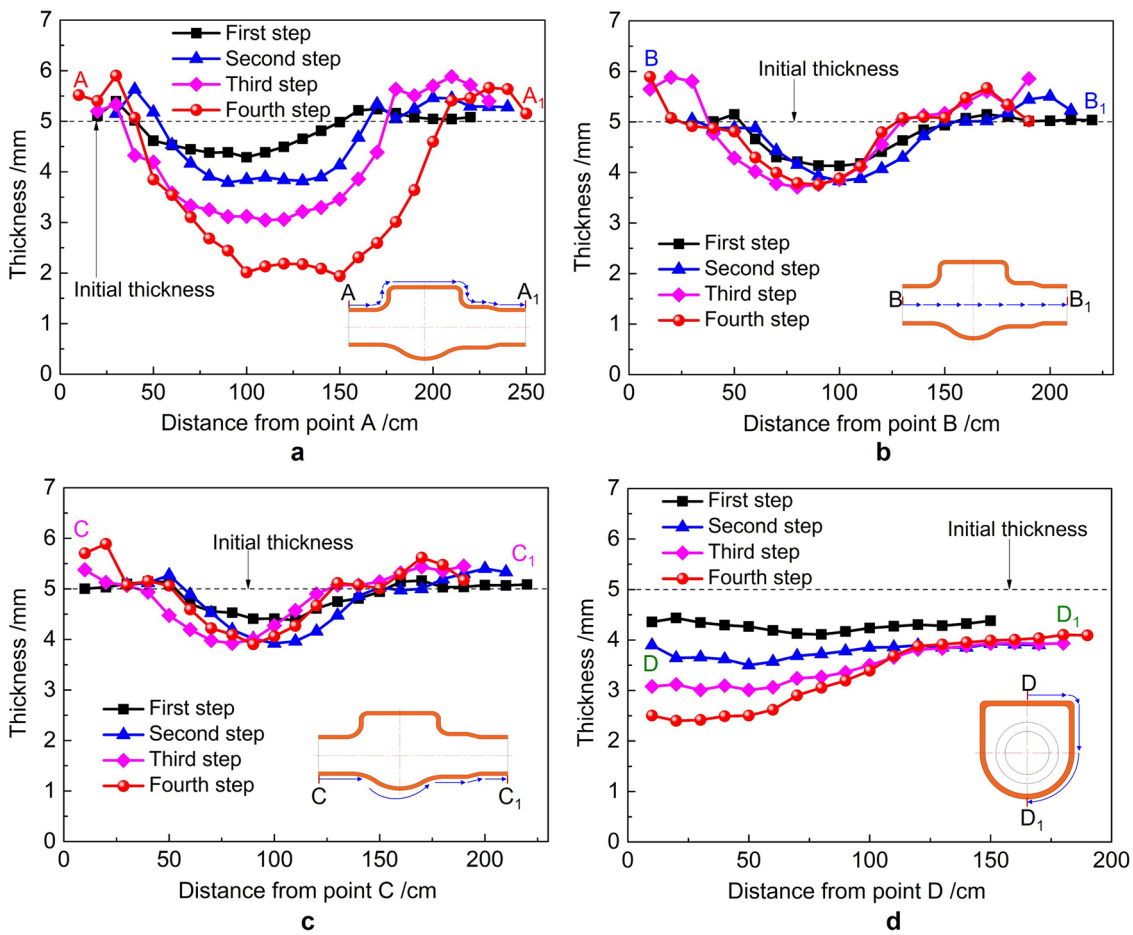

Fig. 7 Thickness distribution of several typical sections on the hydroformed GH4169 T-shaped tubular part: **a** path A-A_1 on the vertical longitudinal section; **b** path B-B_1 on the horizontal longitudinal section; **c** path C-C_1 on the vertical longitudinal section; **d** path D-D_1 on the cross section

path D-D_1, the thickness is always reduced, and the thinnest point is located slightly above the axis intersection point of the main tube and the side branch.

After the second step of hydroforming, the thickness increases more obviously in the transition areas. The main reason is that the material flow direction changes 90° through the transition area from the main tube to the side branch, which will increase the flow resistance and accumulate the material here. On the path A-A_1, the thickness was significantly reduced in the side branch zone due to a greatly bulging, and the maximum thickness thinning point locates between the corner and center of the side branch top. The thickness distributions on the paths of B-B_1 and C-C_1 are basically like that on the path of A-A_1. However, the thickness thinning ratio between the left and right transition areas on the paths B-B_1 and C-C_1 is smaller. On the path D-D_1, the thickness is further reduced compared with that of the first step, and the thinnest point is located at the corner of the side branch top.

In the third step, the thickness at both ends of the tube blank continues to increase on the path A-A_1, while it is further reduced in the side branch zone. A thickness invariant dividing line moves toward the tube ends, so the thickness thinning area is slightly enlarged. On the paths of B-B_1 and C-C_1, the thickness at tube ends is further thickened, while it is almost unchanged between the transition areas at both sides. The thickness invariant dividing line moves toward the center of the side branch, thus the thickness thinning area is reduced. On the D-D_1 path, the thickness in the hemisphere zone did not change compared with that in the second step, and the thinnest point has shifted to the top of the side branch.

After the fourth hydroforming step, the thickness invariant dividing line on the A-A_1 path further moves toward the tube ends, and the thickness thinning area is further enlarged. At the same time, the thickness of the side branch zone is further thinned, where the minimum thickness is 1.939 mm. The thickness distributions on the paths of B-B_1 and C-C_1 are almost the same as that in the third step. Furthermore, on the path of D-D_1, the thickness in the hemisphere zone did not change, but it is further reduced in the side branch.

Figure 8 shows a contour map of the thickness variation in the four-step hydroforming process from the numerical simulation results. It can be seen from Fig. 8 that the thickness thinning and thickening areas, as well as the movements of the thickness invariant dividing line, are consistent with the experimental results in Fig. 7.

4 Discussion

It is known that different stress states occur in the tube blank under different matching conditions of axial feeding length and internal pressure in the hydroforming process, and the thickness variation trend is closely related to the stress state [21]. According to a sequential correspondence law between stress and strain components [22], if the magnitude sequence of the stresses $\sigma_1 > \sigma_2 > \sigma_3$ and the associated principal axes of strain remain unchanged during the plastic deformation process, the sequence of the principal stress components

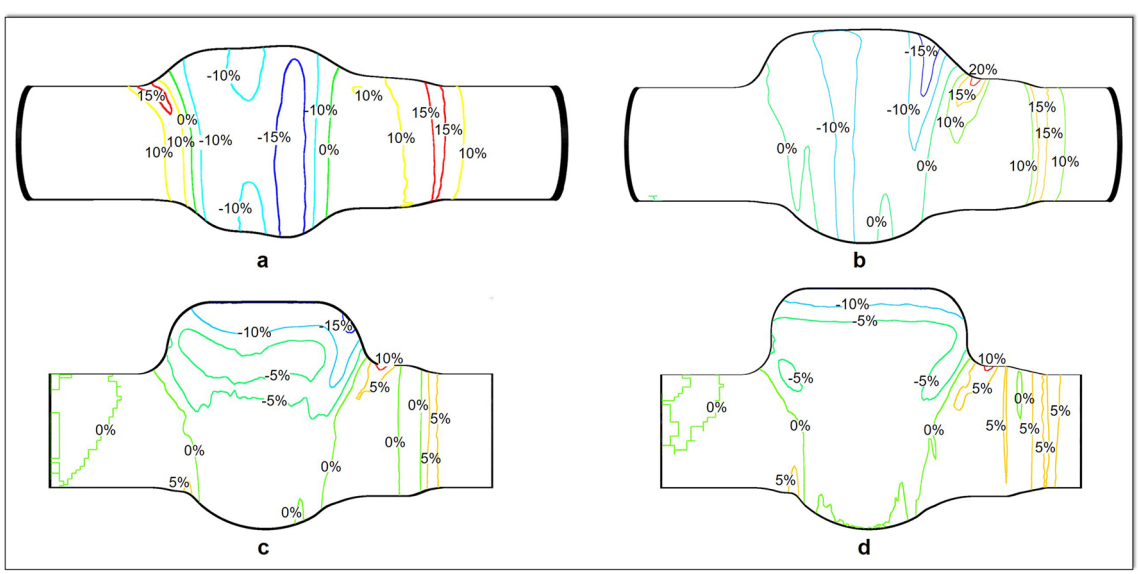

Fig. 8 Contour map of thickness variation ratio of the T-shaped tube in the four-step hydroforming process [8]: **a** first step; **b** second step; **c** third step; **d** forth step

corresponds to the sequence of the principal strain components, viz. $\varepsilon_1 > \varepsilon_2 > \varepsilon_3$ ($\varepsilon_1 > 0,\ \varepsilon_3 < 0$). Furthermore, an unchangeable relationship $\sigma_2 \gtreqless \frac{\sigma_1+\sigma_3}{2}$ gives $\varepsilon_2 \gtreqless 0$. Because the Lode parameter can be expressed as: $\mu_\sigma = \frac{2\sigma_2-(\sigma_1+\sigma_3)}{\sigma_1-\sigma_3}$. Therefore, the deformation type is related to the Lode parameter μ_σ. When $\mu_\sigma > 0$, a compression deformation will be generated; when $\mu_\sigma < 0$, an elongation deformation will be produced; moreover, the $\mu_\sigma = 0$ corresponds to a plane strain deformation [23].

In the four-step hydroforming process of complex nickel-based superalloy T-shaped tubular part, let the three principal stresses be σ_θ, σ_z and σ_t, respectively, and $\sigma_\theta > 0$, $\sigma_t < 0$, then the thickness variation trend completely depends on the relative magnitude of axial stress σ_z and normal stress σ_t. It can be mainly divided into following cases:

(1) When the axial direction is subjected to great compressive stress, i.e., $\sigma_\theta > \sigma_t > \sigma_z$, the Lode parameter can be expressed as $\mu_\sigma = \frac{2\sigma_t-(\sigma_\theta+\sigma_z)}{\sigma_\theta-\sigma_z}$, then:

- If $\sigma_t > (\sigma_\theta + \sigma_z)/2$, $\mu_\sigma > 0$, the compressive deformation will be generated, and $d\varepsilon_t > 0$, which corresponds to a thickness thickening;
- If $\sigma_t = (\sigma_\theta + \sigma_z)/2$, $\mu_\sigma = 0$, the plane strain deformation will occur, and $d\varepsilon_t = 0$, which indicates the thickness will remain constant;
- Else if $\sigma_t < (\sigma_\theta + \sigma_z)/2$, $\mu_\sigma < 0$, the elongation deformation will be produced, and $d\varepsilon_t < 0$, which results to a thickness reduction.

It can be seen from above that there is a one-to-one correspondence between the Lode parameter μ_σ and the thickness variation trend when the through-thickness normal stress σ_t is the middle principal stress.

(2) When there is no axial stress or the axial direction is subjected to less compressive stress or tensile stress, i.e., $\sigma_\theta > \sigma_z > \sigma_t$, then the Lode parameter can be expressed as $\mu_\sigma = \frac{2\sigma_z-(\sigma_\theta+\sigma_t)}{\sigma_\theta-\sigma_z}$. In this case, $d\varepsilon_t < 0$ is always true no matter how the Lode parameter μ_σ changes, which indicates that the thickness is thinning.

Therefore, the thickness variation at a certain position of the T-shaped tubular part can be judged according to the stress state during the multi-step hydroforming process. Table 4 shows the stress state and thickness variation in left transition area (the corner area between the main tube and side branch) of the complex T-shaped tubular part obtained by numerical simulation results and calculation. In the first hydroforming step, the left transition area is in a triaxial compressive stress state. It can be deduced that the left transition area is thickened by substituting the three principal stress components into the sequential correspondence law between stress and strain components. It can be seen from Figs. 7a, 8a that the thickness thickening in the left transition area is about 10–15% at the end of the first hydroforming step, at which the thickness invariant dividing line is located on the wall of the side branch.

In the second step, the compressive circumferential stress and axial stress in the left transition area decrease. The thickness in the left transition area continues to thicken, and the thickness invariant dividing line is still located on the left wall of the side branch. Figure 9 shows the strain distribution in the left transition area of side branch measured by the grid analysis method after the second step of hydroforming experiment. It can be seen from Fig. 9 that the normal strain decreases gradually from the transition area to the top of the side branch, and there is a thickness invariant dividing line on the wall of the side branch where the normal strain is zero, as shown in Fig. 9d.

In the third and fourth steps of hydroforming, the axial stress in the left transition area of the side branch changes into tensile stress, and the thickness is reduced. This will make the thickness invariant dividing line move toward to the tube end, thus the left transition area of the side branch enters the thickness thinning area. The same results can also

Table 4 Stress state and thickness variation in left transition area of side branch of the complex T-shaped tubular part

Hydroforming step number	1	2	3	4
Stress state	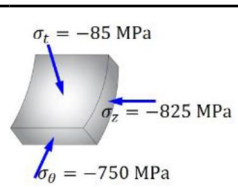	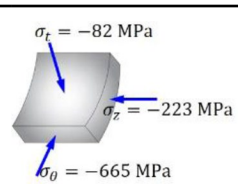	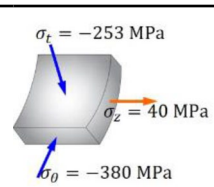	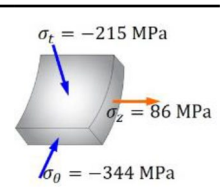
Sequence of stress components	$\sigma_t > \sigma_\theta > \sigma_z$	$\sigma_t > \sigma_z > \sigma_\theta$	$\sigma_z > \sigma_t > \sigma_\theta$	$\sigma_z > \sigma_t > \sigma_\theta$
Sequence of strain components	$\varepsilon_t > \varepsilon_\theta > \varepsilon_z$ $\varepsilon_t > 0,\ \varepsilon_\theta < 0,\ \varepsilon_z < 0$	$\varepsilon_t > \varepsilon_z > \varepsilon_\theta$ $\varepsilon_t > 0,\ \varepsilon_z < 0,\ \varepsilon_\theta < 0$	$\varepsilon_z > \varepsilon_t > \varepsilon_\theta$ $\varepsilon_z < 0,\ \varepsilon_t > 0,\ \varepsilon_\theta < 0$	$\varepsilon_z > \varepsilon_t > \varepsilon_\theta$ $\varepsilon_z < 0,\ \varepsilon_t > 0,\ \varepsilon_\theta < 0$
Thickness variation	Thickening	Thickening	Thinning	Thinning

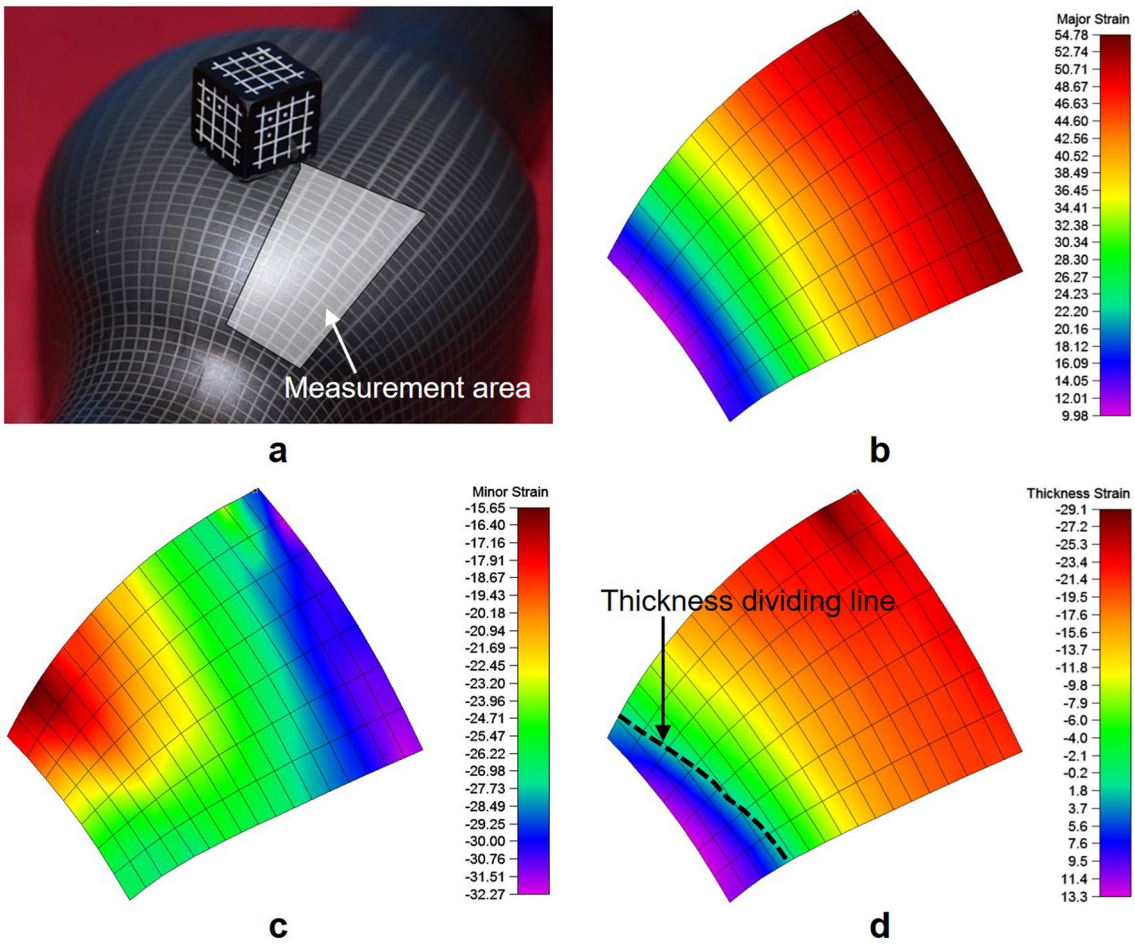

Fig. 9 Strain distribution in the left transition area of side branch after the second hydroforming step: **a** measurement area; **b** major strain; **c** minor strain; **d** thickness strain

be found from Figs. 7a, 8c, d. Figure 10 shows the strain distribution in the left transition area of the side branch after the fourth step of hydroforming experiment. It can be seen from Fig. 10 that the maximum principal strain on the wall of the side branch increases gradually from 11.20 to 58.84%, while the minimum principal strain remains low and varies from − 6.79 to 4.76%. For the normal strain, it varies from − 14.3 to − 54.1%. All the normal strain are negative values, indicating that the left transition area of the side branch is thinning.

Table 5 gives the stress state and thickness variation in top area of the side branch during the four-step hydroforming process obtained by numerical simulation results and calculation. It can be seen from Table 5 that the top of the side branch has not contacted with the middle punch at the end of the first hydroforming step. At this moment, the stress state can be simplified to a plane stress state. According to the sequential correspondence law between stress and strain components, it can be concluded that the thickness thins during the first hydroforming step. From the second step of hydroforming, the top of the side branch is in contact with the middle punch. Therefore, the normal stress cannot be ignored, and the stress state changes into a 3D stress state with two-direction tension and one-direction compression, in which the normal stress is the minimum principal stress. Therefore, no matter how the relationship between circumferential stress and axial stress changes, the thickness always decreases.

Figures 11, 12 show the strain distribution in the top area of side branch after the third and fourth steps of hydroforming experiment. Clearly, after the third step, the deformation on the top of the side branch are very uniform. The maximum strain is between 67.34 and 68.94%, while the minimum principal strain is between − 27.40 and − 24.32%. For the normal strain, it varies from − 44.0 to − 41.4%, which indicates that the thickness has thinned. When the fourth step is finished, the thickness at the top of the side branch is further reduced.

Table 6 gives the stress state and thickness variation at pole of the hemisphere zone in the four-step hydroforming

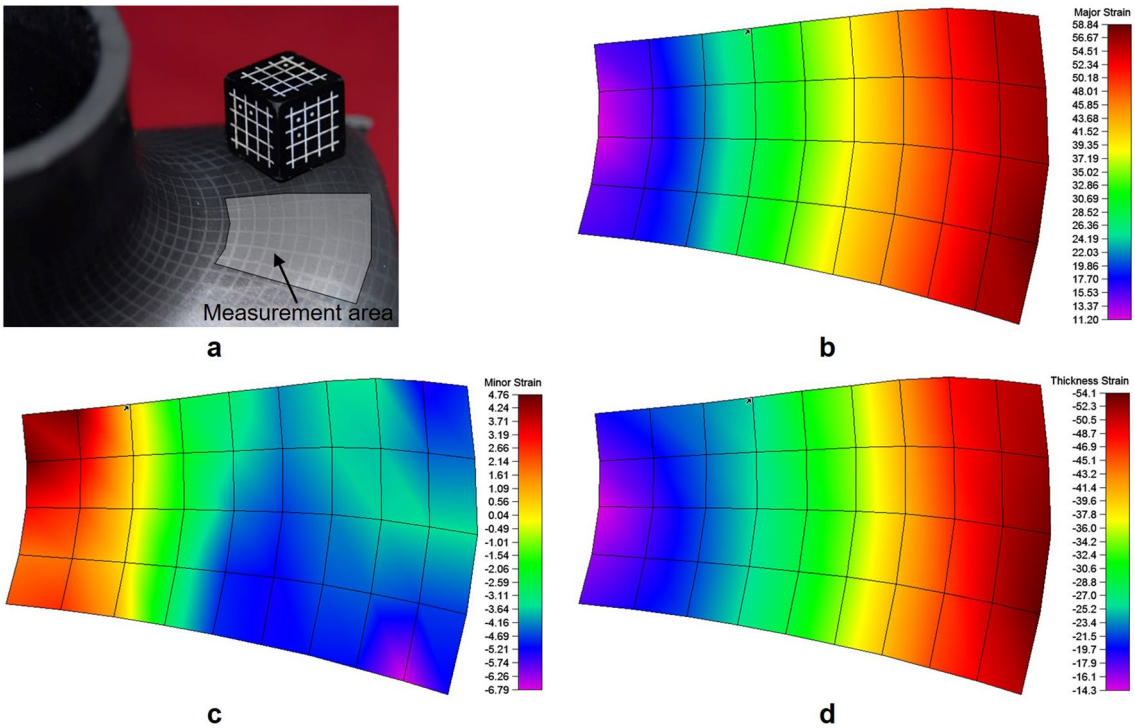

Fig. 10 Strain distribution in the left transition area of side branch after the fourth hydroforming step: **a** measurement area; **b** major strain; **c** minor strain; **d** thickness strain

Table 5 Stress state and thickness variation in top area of side branch of the complex T-shaped tubular part

Hydroforming step number	1	2	3	4
Stress state	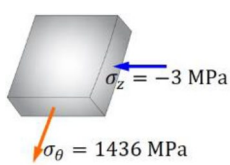	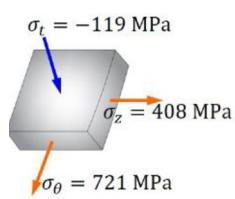	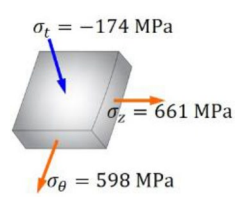	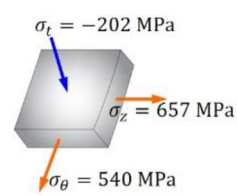
Sequence of stress components	$\sigma_\theta > \sigma_t > \sigma_z$	$\sigma_\theta > \sigma_z > \sigma_t$	$\sigma_z > \sigma_\theta > \sigma_t$	$\sigma_z > \sigma_\theta > \sigma_t$
Sequence of strain components	$\varepsilon_\theta > \varepsilon_t > \varepsilon_z$ $\varepsilon_\theta < 0, \varepsilon_t > 0,\ \varepsilon_z < 0$	$\varepsilon_\theta > \varepsilon_z > \varepsilon_t$ $\varepsilon_\theta < 0, \varepsilon_z < 0, \varepsilon_t > 0,$	$\varepsilon_z > \varepsilon_\theta > \varepsilon_t$ $\varepsilon_z < 0, \varepsilon_\theta < 0,\ \varepsilon_t > 0$	$\varepsilon_z > \varepsilon_\theta > \varepsilon_t$ $\varepsilon_z < 0, \varepsilon_\theta < 0,\ \varepsilon_t > 0$
Thickness variation	Thinning	Thinning	Thinning	Thinning

process obtained by numerical simulation results and calculation. It can be seen from Table 6 that in each step of the hydroforming process, the pole of hemisphere zone is subjected to compressive axial stress and tensile circumferential stress. In the first step of hydroforming, it is subjected to a great circumferential stress of 1305 MPa, under which the circumferential strain reaches 52.7% and the thickness is reduced by 11.9%. In the subsequent hydroforming steps, the hemisphere zone adheres to the die cavity, and the tensile circumferential stress received at the pole decreases. Therefore, the thickness thinning at the pole of hemisphere zone decreases gradually. In the fourth step, almost no plastic deformation occurred in the thickness direction. This is agreement with the variation rule of thickness distribution measured in experiment shown in Fig. 7c. In brief, the thickness variation of the superalloy GH4169 T-shaped tubular part with expanded diameter is very complex during the four-step hydroforming process. The stress state at a certain position can be used to qualitatively predict the thickness variation trend according to the sequential correspondence law between stress and strain components.

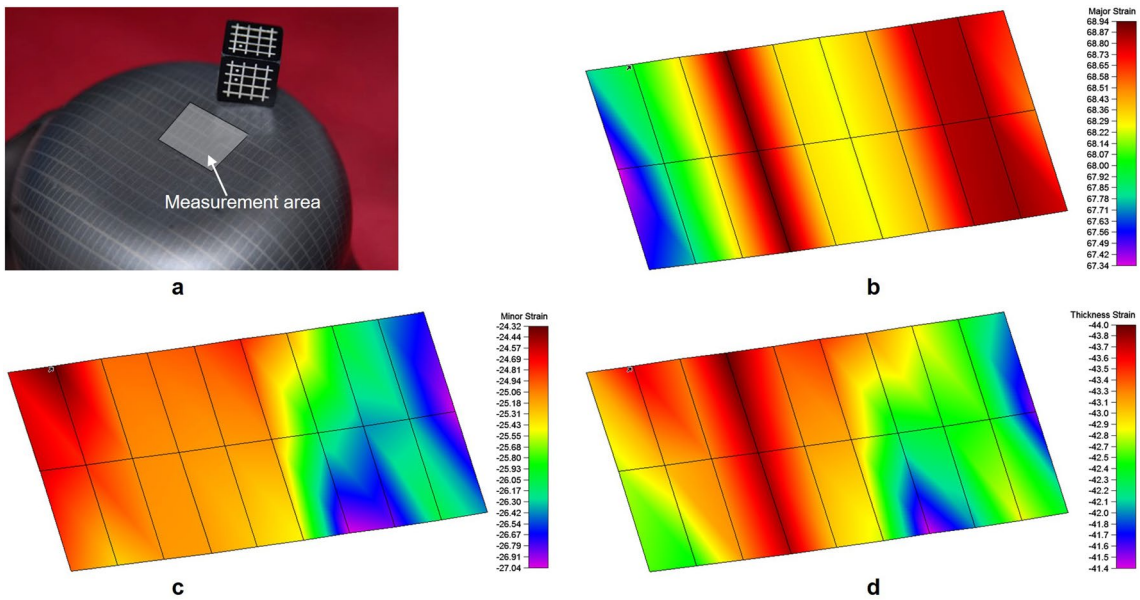

Fig. 11 Strain distribution in the top area of side branch after the third hydroforming step: **a** measurement area; **b** major strain; **c** minor strain; **d** thickness strain

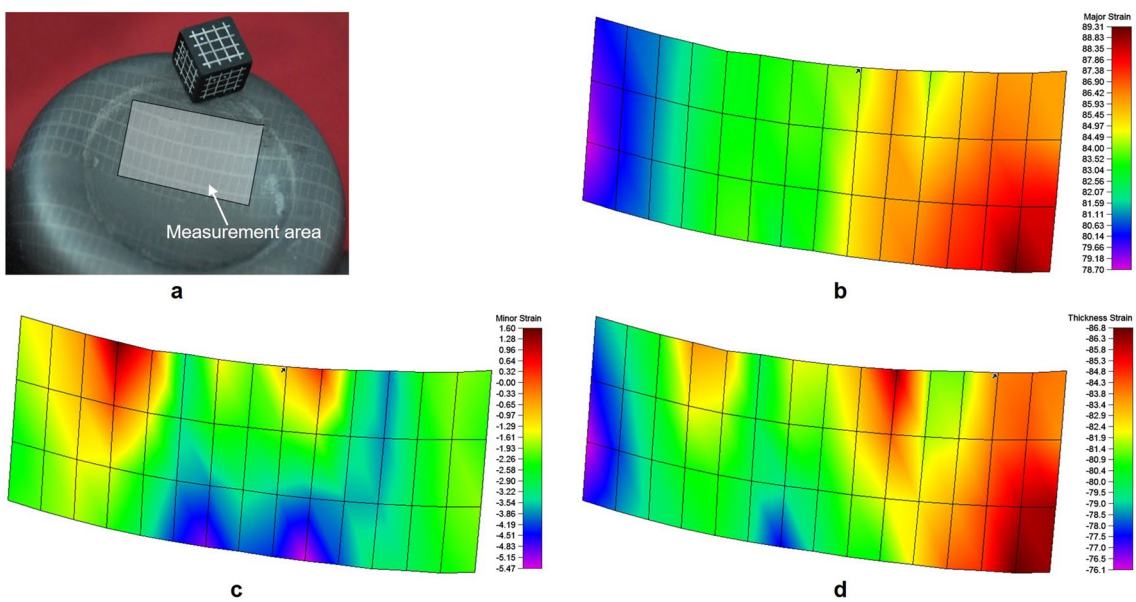

Fig. 12 Strain distribution in the top area of side branch after the fourth hydroforming step: **a** measurement area; **b** major strain; **c** minor strain; **d** thickness strain

5 Conclusions

In this investigation, the thickness variation and stress state of a GH4169 T-shaped tubular part with expanded diameter have been analyzed in four-step hydroforming process. Conclusions can be drawn from this work as follows:

1. The flow trajectories of typical points on the tubular part were analyzed to reveal the material flow behavior. It is found that material flow at the top of side branch occurs in a large space, and they have the different flow directions to form the left corner, the center, the right corner and the front corner.

Table 6 Stress state and thickness variation at pole of hemisphere zone of the complex T-shaped tubular part

Hydroforming step number	1	2	3	4
Stress state	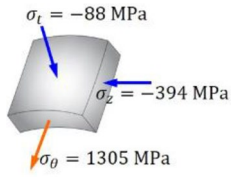	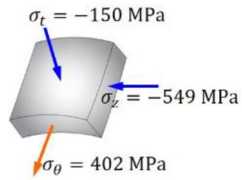	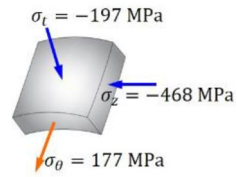	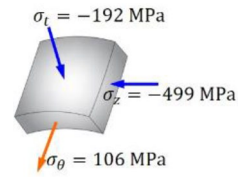
Sequence of stress components	$\sigma_\theta > \sigma_t > \sigma_z$	$\sigma_\theta > \sigma_t > \sigma_z$	$\sigma_\theta > \sigma_t > \sigma_z$	$\sigma_\theta > \sigma_t > \sigma_z$
Sequence of strain components	$\varepsilon_\theta > \varepsilon_t > \varepsilon_z$ $\varepsilon_\theta < 0, \varepsilon_t > 0,\ \varepsilon_z < 0$	$\varepsilon_\theta > \varepsilon_t > \varepsilon_z$ $\varepsilon_\theta < 0, \varepsilon_t > 0,\ \varepsilon_z < 0$	$\varepsilon_\theta > \varepsilon_t > \varepsilon_z$ $\varepsilon_\theta < 0, \varepsilon_t > 0,\ \varepsilon_z < 0$	$\varepsilon_\theta > \varepsilon_t > \varepsilon_z$ $\varepsilon_\theta < 0, \varepsilon_t > 0,\ \varepsilon_z < 0$
Thickness variation	Thinning	Thinning	Thinning	Unchanged

2. The thickness variations of the GH4169 T-shaped tubular part in four-step hydroforming process are discussed. Due to a large axial feeding, the material accumulates in the transition area on both sides of the side branch, which induce the continuous thickening between the transition areas and the tube ends in all hydroforming steps. At the same time, the side branch zone is always thinned during the four-step hydroforming process, and the minimum thickness is 1.939 mm which is in the area between the center and the corner of the side branch top. For other deformation zones, they are only thinned in the first step, and their thickness changed little in the subsequent forming steps.
3. In the four-step hydroforming of the GH4169 T-shaped tubular part, the thickness invariant dividing line in the side branch zone first locates on its wall, then it moves toward the tube ends with forming going on. Thus, the thickness thinning area is enlarged. However, in the hemisphere zone, the thickness invariant dividing line moves slightly towards the center of the side branch, and the thickness reduction area becomes smaller.
4. The thickness variations at three typical positions of the left transition area, the top area of side branch and the pole of hemisphere zone, as well as their relationship with the stress state, are analyzed using the sequential correspondence law between stress and strain components. On this basis, the mechanism of thickening in the left transition area, thinning at the top of side branch and thickness variation at the hemispheric pole was revealed.

Acknowledgements This investigation is financially supported by the National Natural Science Foundation of China (Number U1937205, 51805357), the Project Funded by China Postdoctoral Science Foundation (Number 2020M670907), and the Project Supported by Heilongjiang Postdoctoral Foundation (Number LBH-Z20017). The authors wish to express their gratitude to the funding support. The authors also would like to thank for the contributions of Xiaohui Lu to the experiments.

Declarations

Conflict of interest The authors declare that they have no conflict of interest.

References

1. Mouritz AP, editor. Superalloys for gas turbine engines. Introduction to aerospace materials. Amsterdam: Elsevier; 2012. p. 251–67. https://doi.org/10.1533/9780857095152.251.
2. Bell C, Corney J, Zuelli N, Savings D. A state of the art review of hydroforming technology. Int J Mater Form. 2020;13:789–828. https://doi.org/10.1007/s12289-019-01507-1.
3. Ray P, Mac Donald BJ. Experimental study and finite element analysis of simple X- and T-branch tube hydroforming processes. Int J Mech Sci. 2005;47:1498–518. https://doi.org/10.1016/j.ijmecsci.2005.06.007.
4. Crapps J, Marin EB, Horstemeyer MF, Yassar R, Wang PT. Internal state variable plasticity-damage modeling of the copper tee-shaped tube hydroforming process. J Mater Process Technol. 2010;210:1726–37. https://doi.org/10.1016/j.jmatprotec.2010.06.003.
5. Kashani Zadeh H, Mashhadi MM. Finite element simulation and experiment in tube hydroforming of unequal T shapes. J Mater Process Technol. 2006;177:684–7. https://doi.org/10.1016/j.jmatprotec.2006.04.056.
6. Hwang Y-M, Wang K-H, Kang N-S. Adaptive simulations in T-shape tube hydroforming with different outlet diameters. Proc Inst Mech Eng. 2015;229:597–608. https://doi.org/10.1177/0954405413519609.
7. Hwang Y-M, Wang K-H, Kang N-S. T-shape tube hydroforming of magnesium alloys with different outlet diameters. J Manuf Sci Eng. 2011;133: 061012. https://doi.org/10.1115/1.4004851.
8. Cui X-L, Teng B, Yuan S. Hydroforming process of complex T-shaped tubular parts of nickel-based superalloy. CIRP J Manuf Sci Technol. 2020;32:476–90. https://doi.org/10.1016/j.cirpj.2021.02.001.
9. Yuan S. Fundamentals and processes of fluid pressure forming technology for complex thin-walled components. Engineering. 2020;7(3):358–66. https://doi.org/10.1016/j.eng.2020.08.014.

10. Cheng DM, Teng BG, Guo B, Yuan SJ. Thickness distribution of a hydroformed Y-shape tube. Mater Sci Eng A. 2009;499:36–9. https://doi.org/10.1016/j.msea.2007.09.100.
11. Ahmetoglu M, Sutter K, Li X, Altan T. Tube hydroforming: current research, applications and need for training. J Mater Process Technol. 2000;98:224–31. https://doi.org/10.1016/S0924-0136(99)00203-4.
12. Guo XZ, Tao J, Yuan Z, Tang QS. Hydroforming simulation and preparation of low activation martensitic steel Y-shapes. Nucl Eng Des. 2011;241:2802–6. https://doi.org/10.1016/j.nucengdes.2011.06.006.
13. Peng J, Zhang W, Liu G, Zhu S, Yuan S. Effect of internal pressure distribution on thickness uniformity of hydroforming Y-shaped tube. Trans Nonferrous Met Soc China. 2011;21:s423–8. https://doi.org/10.1016/S1003-6326(11)61618-X.
14. Hwang Y-M, Su Y-H, Chen B-J. Tube hydroforming of magnesium alloys at elevated temperatures. J Eng Mater Technol. 2010;132: 031012. https://doi.org/10.1115/1.4001833.
15. Hwang YM, Wang KH. Study on Y-shape tube hydroforming of magnesium alloys at elevated temperatures. Int J Mater Form. 2010;3:175–8. https://doi.org/10.1007/s12289-010-0735-y.
16. Lei L-P, Kim J, Kang B-S. Bursting failure prediction in tube hydroforming processes by using rigid-plastic FEM combined with ductile fracture criterion. Int J Mech Sci. 2002;44:1411–28. https://doi.org/10.1016/S0020-7403(02)00045-0.
17. Di Lorenzo R, Ingarao G, Chinesta F. Integration of gradient based and response surface methods to develop a cascade optimisation strategy for Y-shaped tube hydroforming process design. Adv Eng Softw. 2010;41:336–48. https://doi.org/10.1016/j.advengsoft.2009.06.010.
18. Rajenthirakumar D. Experimental and numerical investigations on sheet and tube hydroforming of inconel alloy. Chennai: Anna University; 2010. p. 625.
19. Academic Committee of the Superalloys. The Chinese Society for Metals (ed). China superalloys handbook, 1st edn. Beijing: China Quality and Standards Publishing and Media Co. Ltd; 2012. p. 690.
20. An XL, Zhang B, Chu CL, Zhou L, Chu PK. Evolution of microstructures and properties of the GH4169 superalloy during short-term and high-temperature processing. Mater Sci Eng A. 2019;744:255–66. https://doi.org/10.1016/j.msea.2018.12.019.
21. Li HY, Wang XS, Yuan SJ, Miao QB, Wang ZR. Typical stress states of tube hydroforming and their distribution on the yield ellipse. J Mater Process Technol. 2004;151:345–9. https://doi.org/10.1016/j.jmatprotec.2004.04.085.
22. Wang Z, Hu W, Yuan SJ, Wang X. Sequential correspondence law between stress and strain components and its application in plastic deformation process, in: Engineering Plasticity: Theory and Applications in Metal Forming. Singapore: John Wiley and Sons Singapore Pte. Ltd; 2018. p. 295–316. https://doi.org/10.1002/9781119237310.ch7.
23. Wang Z. Physical essence of Lode parameter and its effect of plastic flow. Acta Mech Solida Sin (Chinese). 2006;27:277–82. https://doi.org/10.19636/j.cnki.cjsm42-1250/o3.2006.03.010.

Publisher's Note Springer Nature remains neutral with regard to jurisdictional claims in published maps and institutional affiliations.

Authors and Affiliations

Xiao-Lei Cui[1,2] · Shijian Yuan[1]

✉ Shijian Yuan
syuan@hit.edu.cn

Xiao-Lei Cui
xiaoleicui@hit.edu.cn

[1] National Key Laboratory for Precision Hot Processing of Metals, Harbin Institute of Technology, Harbin 150001, China

[2] School of Materials Science and Engineering, Harbin Institute of Technology, Harbin 150001, China